

The impact of temporal sampling resolution on parameter inference for biological transport models

Jonathan U. Harrison*¹, Ruth E. Baker¹,

¹ Wolfson Centre for Mathematical Biology, Mathematical Institute, University of Oxford, United Kingdom

* harrison@maths.ox.ac.uk

Abstract

Imaging data has become widely available to study biological systems at various scales, for example the motile behaviour of bacteria or the transport of mRNA, and it has the potential to transform our understanding of key transport mechanisms. Often these imaging studies require us to compare biological species or mutants, and to do this we need to quantitatively characterise their behaviour. Mathematical models offer a quantitative description of a system that enables us to perform this comparison, but to relate these mechanistic mathematical models to imaging data, we need to estimate the parameters of the models. In this work, we study the impact of collecting data at different temporal resolutions on parameter inference for biological transport models by performing exact inference for simple velocity jump process models in a Bayesian framework. This issue is prominent in a host of studies because the majority of imaging technologies place constraints on the frequency with which images can be collected, and the discrete nature of observations can introduce errors into parameter estimates. In this work, we avoid such errors by formulating the velocity jump process model within a hidden states framework. This allows us to obtain estimates of the reorientation rate and noise amplitude for noisy observations of a simple velocity jump process. We demonstrate the sensitivity of these estimates to temporal variations in the sampling resolution and extent of measurement noise. We use our methodology to

provide experimental guidelines for researchers aiming to characterise motile behaviour that can be described by a velocity jump process. In particular, we consider how experimental constraints resulting in a trade-off between temporal sampling resolution and observation noise may affect parameter estimates.

Author summary

We consider how the temporal resolution of imaging studies affects our ability to carry out accurate parameter estimation for a stochastic biological transport model. This model provides a mechanistic description of motile behaviour and is often used to interrogate transport processes, such as the motion of bacteria. Parameter inference is necessary to characterise different types of transport and to make predictions about biological behaviour under different conditions. Typically, observations of the transport process, at the level of individual trajectories, are made at discrete times. This can lead to errors in parameter estimation because we do not have complete trajectory information. We present a framework for Bayesian inference for these models of biological transport processes. Using this framework, we study the effects of collecting data more or less frequently, and with varying measurement noise, on what we can learn about the biological system via parameter estimation.

Introduction

Biological transport processes occur on a wide range of spatial and temporal scales, but a common mechanism for transport involves two phases: fast active transport, and a quasi-stationary reorientation phase. This pattern of movements has been observed at a range of scales from the intracellular transport of cellular components such as mRNA particles moving on a microtubular network [29], to the run-and-tumble motion of bacteria such as *Escherichia coli* [6, 25, 32], and the flights of birds between nesting sites [36]. To capture appropriately these two phases of motion, a class of models known as velocity jump process (VJP) models [10, 11, 25, 26, 36] (also known as correlated random walks [9, 19–22] or Levy Walks [5, 13, 38, 39]) have been developed.

Estimating the parameters of these models can inform us about mechanistic

parameters relating to the underlying biological process, such as the rate of reorientation. Being able to obtain accurate estimates, with appropriate uncertainty, for these parameters allows us to compare different biological species or mutants, and gain an understanding of the underlying mechanistic behaviour. Importantly, parameterising models, and quantifying the uncertainty in parameter estimates, as can be achieved via Bayesian inference, enables us to use models to make quantitative predictions of behaviour in new conditions, with quantifiable uncertainty. By performing experiments to test model predictions, we can evaluate the areas in which a given model fails to describe the experimental data, and so iteratively refine our understanding of a given system or phenomenon.

In this work, we consider the effects that experimental design can have on the information we can obtain from a data set, in terms of using that data to estimate parameters of a computational model. In particular, for time series data describing a biological transport process, we vary the time between successive measurements. We demonstrate a framework for estimating the parameters of a VJP model for data of this form in the presence of noise, and examine how the posterior estimates of the model parameters change for more coarsely sampled and noisier datasets. Our framework formulates the VJP model as a process with hidden states, as in a hidden Markov model (HMM), which allows us to use particle Markov Chain Monte Carlo (pMCMC) methods to perform exact Bayesian inference. We use our framework to suggest sensible experimental design choices in the context of microscopy studies, where there may be a trade-off between how frequently it is possible to image, and the noise resulting from more or less frequent observations of the process. Finally, we present a comparison between the pMCMC framework described in this work and approximate Bayesian computation (ABC) for parameter inference in this context.

Velocity jump process models

VJP models have been developed to describe biological transport processes where there is persistent or biased random motion [25, 27, 36]. Correlated, persistent motion is observed experimentally in a variety of contexts [23, 28]. VJP models are most appropriate for motion consisting of multiple phases such as a fast directed phase and

a stationary or reorientation phase, and these models describe how an object moves in one direction before reorienting and moving in a new direction. This type of “run and reorientate” motion is exhibited, for example, by *Escherichia coli* [6, 32], fibroblasts [28], and RNA-protein complexes [29].

We present here a mathematical description of a VJP model. Suppose we have a running time distribution, with probability density function (pdf) f_τ , and a waiting time distribution, with pdf f_μ . Random variables drawn from these distributions dictate the lengths of time spent in the fast active transport, or running phase of the VJP and the reorientation phase, respectively. After the reorientation phase, a direction for the new run is chosen according to a reorientation kernel, f_Φ . For biological processes with a distinct separation of timescales between these two phases, it is often possible to assume that reorientations between successive runs occurs instantaneously and therefore neglect the reorientation phase in a model of the process [25, 36]. This results in simulated trajectories as shown in Fig 1.

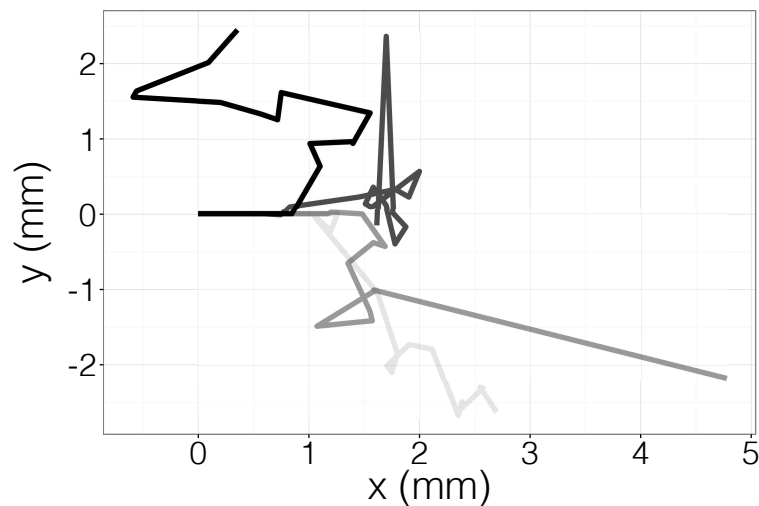


Fig 1. Four example VJP trajectories, simulated with a uniform reorientation kernel, reorientation frequency $\lambda = 0.2 \text{ s}^{-1}$ and running speed $c = 50 \mu\text{ms}^{-1}$ for a duration of $T = 64 \text{ s}$. These trajectories start from the origin, and are orientated initially parallel to the positive x -axis.

In the simplest case, where we assume that the running time distribution is memoryless, that is, exponentially distributed, with $f_\tau(t) = \lambda \exp(-\lambda t)$, the long time behaviour of the mean squared displacement scales linearly with time, t [25]. Further moments of the motion of individuals displaying such VJP behaviour have been

characterised by making certain closure assumptions [10]. For the case of a more general running time distribution, with finite mean and variance, in the large time limit, the probability of the particle being at position x at time t follows a diffusion equation [36].

In practice, VJP models are often parameterised by obtaining measurements of the effective diffusion coefficient or the mean squared displacement, and using these data to estimate the parameters of a specific running distribution [25, 36]. Rosser et al. [32] parameterised a HMM via maximum likelihood estimation, whilst Nicosia et al. [24] fitted a hidden state random walk model to animal movement data using an expectation-maximization algorithm. These frequentist approaches can provide useful point estimates of the VJP parameters, but fail to take account of the uncertainty inherent in these estimates which can be crucial when dealing with noisy biological data (see Fig 1). By adopting a Bayesian approach to parameter estimation, in this work we are able to obtain a posterior distribution for model parameters of interest, which gives a quantifiable uncertainty to estimates. These quantitative measures of uncertainty enable the generation of predictions of further biological behaviour using the model, and characterisation of their uncertainty. In addition, we can consider the effects of noisy data measurements upon the accuracy of parameter inference, which has previously been difficult to deal with in practice, or has been neglected.

For simplicity, in this work we will assume that there is a separation of timescales between running and reorientation phases, such that reorientations can be considered instantaneous. In addition, we assume that the running time distribution, f_τ , is exponentially distributed and the reorientation kernel is a uniform distribution on $[-\pi, \pi)$. We follow the trajectory of a single, motile individual, and take, as experimental measurements, the change in angle between successive observed positions (calculated relative to the previous observed position), subject to measurement noise drawn from a wrapped Normal distribution, $N(0, \sigma^2)$, where σ is the magnitude of the noise (see Fig 2 where the observed angle change between observations at times $k\Delta t$ and $(k + 1)\Delta t$ is θ_1). Our Bayesian inference approach will target estimation of the reorientation rate, λ , and the magnitude of the noise, σ .

Inference for velocity jump process models via particle Markov chain Monte Carlo

Inference for partially observed Markov processes can be performed using particle Markov Chain Monte Carlo (pMCMC), as developed by Andrieu and Roberts [1] and Andrieu et al. [2]. pMCMC provides a Bayesian framework for parameter estimation by allowing samples to be drawn from the posterior distribution of the model parameters, given observed data, without needing to evaluate the likelihood function directly. For partially observed Markov process models, the model structure makes directly evaluating the likelihood difficult or expensive¹. Instead of evaluating the likelihood directly, we can use (unbiased) estimates of the likelihood within an MCMC algorithm. Estimating the likelihood of the observed data given certain parameters can be achieved with a particle filter (also known as a sequential Monte Carlo scheme) [17] for a fixed, finite, number of particles. The results of Andrieu et al. [2] demonstrate that, even when a finite number of particles are used in the filter to estimate the likelihood, the MCMC algorithm will still target the correct posterior distribution. These methods have been applied in the context of modelling of epidemics [31] and of biochemical reaction networks [15, 16]. However, pMCMC methods for parameter inference have not previously been applied to spatial agent-based models, such as the VJP model considered here. The pMCMC algorithm used in this work is given in Algorithm 1 for an observed dataset $\mathbf{y} = \{y_k \mid k = 1, 2, \dots, T\}$.

Algorithm 1 Particle MCMC

- 1: Initialise parameters, θ_0 .
- 2: Run a particle filter (see Algorithm 2) to compute an estimate of the marginalised likelihood $\hat{p}(\mathbf{y}|\theta_0)$, where \mathbf{y} is the observed data.
- 3: **for** $k = 1 : N$ **do**
- 4: Draw parameters θ^* from a proposal distribution $q(\cdot|\theta_{k-1})$.
- 5: Run a particle filter to compute an estimate of the marginalised likelihood $\hat{p}(\mathbf{y}|\theta^*)$.
- 6: Accept the proposed move with probability α where

$$\alpha = \max \left(1, \frac{\pi(\theta^*)q(\theta_{k-1}|\theta^*)\hat{p}(\mathbf{y}|\theta^*)}{\pi(\theta_{k-1})q(\theta^*|\theta_{k-1})\hat{p}(\mathbf{y}|\theta_{k-1})} \right).$$

If the move is accepted, set $\theta_k = \theta^*$, otherwise set $\theta_k = \theta_{k-1}$.

- 7: **end for**
-

¹We note that VJP models can be viewed in this form by introducing hidden states, as explained in Section “Methods”.

Algorithm 2 Bootstrap particle filter

- 1: Sample a collection of particles $\{x_1^1, \dots, x_1^M\}$ from an initial density $p(x_1)$.
- 2: **for** $i = 1 : M$ **do**
- 3: Compute the weights for each particle, i , via $w_1^i = p(y_1|x_1^i, \theta)$.
- 4: Find the normalised weights

$$\tilde{w}_1^i = \frac{w_1^i}{\sum_{j=1}^M w_1^j}.$$

- 5: **end for**
- 6: Resample N times with replacement from the collection of particles, $\{x_1^1, \dots, x_1^M\}$, with probabilities given by the normalised weights, $\{w_1^1, \dots, w_1^M\}$.
- 7: **for** $t = 1 : (T - 1)$ **do**
- 8: **for** $i = 1 : M$ **do**
- 9: Evolve the current collection of particles according to the forward model, by drawing $x_{t+1}^i \sim p(x_{t+1}|x_t^i, \theta)$.
- 10: Compute the weights for each particle, i , via $w_{t+1}^i = p(y_{t+1}|x_{t+1}^i, \theta)$.
- 11: Find the normalised weights

$$\tilde{w}_{t+1}^i = \frac{w_{t+1}^i}{\sum_{j=1}^M w_{t+1}^j}.$$

- 12: **end for**
- 13: Resample M times with replacement from the collection of particles, $\{x_{t+1}^1, \dots, x_{t+1}^M\}$, with probabilities given by the normalised weights, $\{w_{t+1}^1, \dots, w_{t+1}^M\}$.
- 14: **end for**
- 15: Obtain an estimate of the marginal likelihood using the unnormalised weights, via

$$\hat{p}(\mathbf{y}|\theta) = \prod_{t=1}^T \frac{1}{M} \sum_{i=1}^M w_t^i.$$

- 16: **return** $\hat{p}(\mathbf{y}|\theta)$
-

Details of the bootstrap particle filter algorithm used within pMCMC are given in Algorithm 2. A particle filter represents the state of the system via a population of weighted particles [12]. We obtain an estimate of the likelihood by successively updating the hidden state of the system (represented via the particles) and comparing this hidden state with the observed data at each observed time point, to give new weights for the particles according to how well they match the observed data. To prevent a degenerate situation where the state of the system is represented solely by a single particle, it is necessary to resample from the population of particles according to their weights.

Methods

We will demonstrate how to exploit pMCMC methods to obtain posterior parameter estimates for the VJP outlined in the Introduction by formulating it within an appropriate framework that incorporates hidden states. This formulation additionally allows us to incorporate a model for measurement noise in our observations, as well as explicitly accounting for the temporal discretisation of the data. The hidden states (also known as latent variables) in our model will describe whether or not a reorientation event occurred between observations of the VJP. This is not a variable that we can observe directly, since we only measure the observed angle change. For example, in Fig 2 there was a reorientation event between observations at $t = k\Delta t$ and $t = (k + 1)\Delta t$, and an observed angle change of θ_1 , on the other hand, there was no reorientation event between observations at $t = (k + 1)\Delta t$ and $t = (k + 2)\Delta t$ and an observed angle change of θ_2 . Note that the true reorientation angle for the reorientation event that takes place between observations at $t = k\Delta t$ and $t = (k + 1)\Delta t$ is Φ .

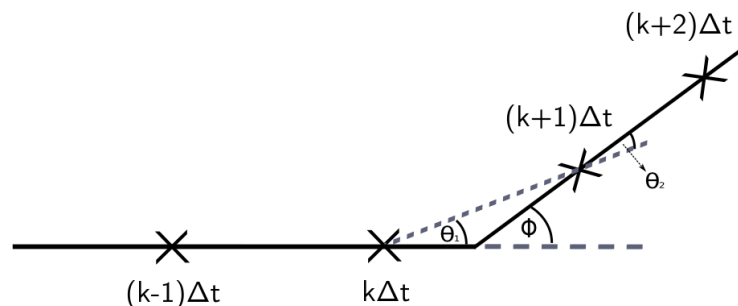


Fig 2. The observed motile individual is observed at discrete times $t = k\Delta t$ for $k \in \{0, 1, \dots, T\}$ (marked by crosses). In each time interval between observations, we measure the angle change between observed the direction of travel between successive observations. We assign a hidden state to each time interval according to whether a reorientation event occurred in that time interval or not. In this example, which excludes measurement noise, there is a reorientation event, through angle Φ , between observations at times $t = k\Delta t$ and $t = (k + 1)\Delta t$; however, the measured angle change between these observations is θ_1 . Conversely, there is no reorientation event between observations at $t = (k + 1)\Delta t$ and $t = (k + 2)\Delta t$ and an observed angle change of θ_2 .

We assume that we observe the system at times $\{k\Delta t : k \in \{0, 1, \dots, T\}\}$ by measuring the position of the individual of interest and recording the observed angle

change. We define the hidden variable, X_k , as follows:

$$X_k = \begin{cases} 1, & \text{if a reorientation event occurred during } [k\Delta t, (k+1)\Delta t), \\ 0, & \text{otherwise.} \end{cases} \quad (1)$$

The observed state is the observed angle change, θ_k , obtained as the difference between the observed direction of travel during $[(k-1)\Delta t, k\Delta t)$ and $[k\Delta t, (k+1)\Delta t)$, $k \geq 1$. We show the hidden and observed states in Fig 3a), with dependence between these states given by the transition and emission probabilities, denoted β_k and p_{ij} , respectively. The hidden variable, X_k , evolves according to the VJP model. Here, since we have an exponential distribution for the running time, $P(\text{reorientation event in } [(k-1)\Delta t, k\Delta t)) = \exp(-\lambda\Delta t)$.

Model without measurement noise

We initially make progress by simplifying the problem and its exposition via the assumption of zero measurement error. To relate the unobserved hidden state to the observed angle change, which we can measure, we derive probability distributions for the angle change given the hidden state. Note that there is additional dependence not only on the current hidden state, but also on the previous hidden states, as shown in Fig. 3b). We can obtain expressions for the emission probabilities by considering the path that is taken under different sequences of hidden states (Fig 4); we will outline simplifying assumptions as they are made.

Suppose we observe the system at times $(k-1)\Delta t, k\Delta t$, and $(k+1)\Delta t$ for some k , as shown in Fig. 4. The sequence of hidden states i, j , correspond to whether there were reorientation events in the time intervals $[(k-1)\Delta t, k\Delta t)$ and $[k\Delta t, (k+1)\Delta t)$ respectively. Let $p_{ij}(\theta)$ be the pdf of observing a reorientation angle of θ given the sequence of hidden states i, j . We assume the angle change θ was observed over the time interval $[k\Delta t, (k+1)\Delta t)$ corresponding to the hidden state j . In the case where no reorientation occurs in either of the time intervals (corresponding to the situation in Fig 4a)), then, assuming no noise, we would observe zero angle change. That is, we have $p_{00}(\theta) = \delta(\theta)$. If a reorientation occurs in the time interval $[k\Delta t, (k+1)\Delta t)$, but not in the preceding time interval, $[(k-1)\Delta t, k\Delta t)$, (as shown in Fig 4b)), then the

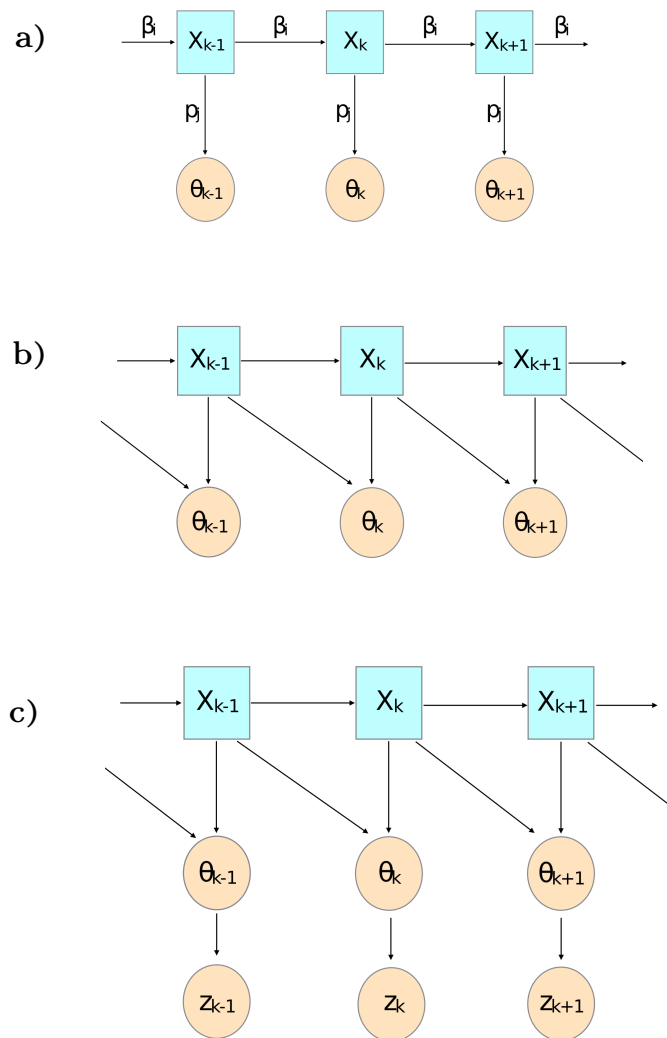


Fig 3. Hidden and observed states in a partially observed Markov process model.

observed reorientation angle is θ_1 , as labelled in Fig 4b). This gives $p_{01}(\theta) := p_{\Theta_1}(\theta)$. The marginal distribution of Θ_1 is derived in the Section “Derivation of emission probabilities”, and depends on the running time distribution and the reorientation kernel.

If, immediately after a reorientation, we have no reorientation in the following time interval, then we may still observe a nonzero angle change since our discrete observation times do not in general coincide with the reorientation events. In this case, we have a reorientation event during $[(k-1)\Delta t, k\Delta t)$, and no reorientation during

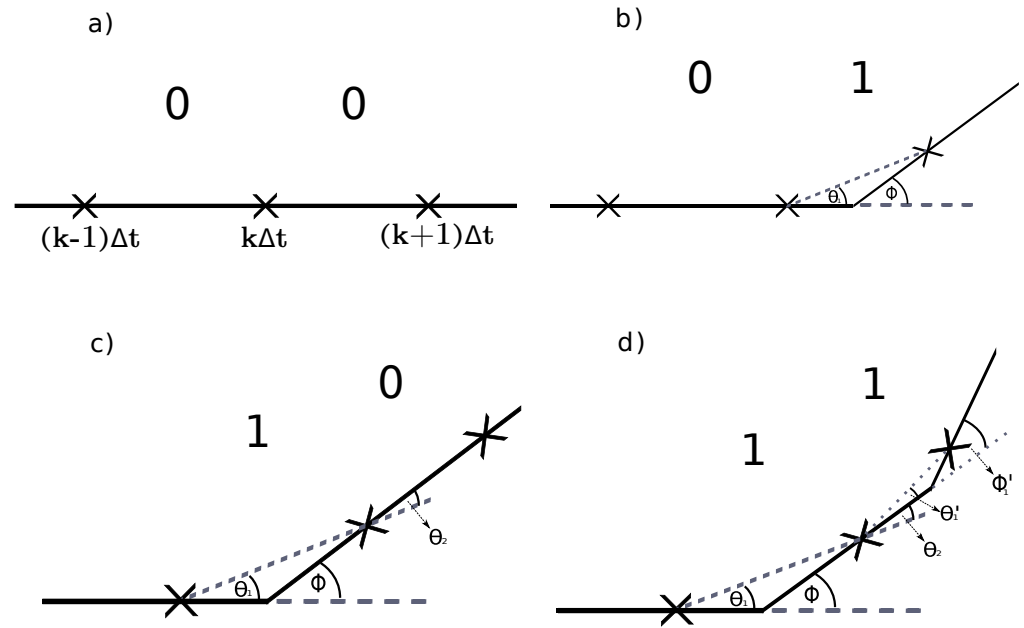


Fig 4. Example paths for each pattern of hidden states. The object of interest moves from left to right, and is observed at times $(k - 1)\Delta t, k\Delta t,$ and $(k + 1)\Delta t$. In a), there are no reorientation events, so the object continues along a straight trajectory. In b), there is a single reorientation in the time interval $[k\Delta t, (k + 1)\Delta t)$, where the object turns through an angle Φ , but the observed angle change is θ_1 due to the discretised observations. In c), there is a single reorientation in the time interval $[(k - 1)\Delta t, k\Delta t)$. The object turns through an angle Φ and continues on its new trajectory. We observe an angle change θ_1 for the time interval $[(k - 1)\Delta t, k\Delta t)$, and observe an angle change θ_2 for the next time interval $[k\Delta t, (k + 1)\Delta t)$ even though there was no reorientation during this time interval. Similarly, in d), there was a reorientation of true angle change Φ during $[(k - 1)\Delta t, k\Delta t)$ followed by another reorientation of true angle change Φ' in the time interval $[k\Delta t, (k + 1)\Delta t)$. In this case, we observe θ_1 for the time interval $[(k - 1)\Delta t, k\Delta t)$, and observe an angle change of $\theta_2 + \theta_1'$ for the time interval $[k\Delta t, (k + 1)\Delta t)$.

$[k\Delta t, (k + 1)\Delta t)$. Such a situation with a pattern of hidden states 1, 0 is shown in Fig 4c), and the observed angle change during the time interval $[k\Delta t, (k + 1)\Delta t)$ corresponds to θ_2 in the diagram. We note that, by geometric arguments, we have

$$\theta_1 + \theta_2 = \Phi, \tag{2}$$

where Φ is the true angle change. Therefore, given a pattern of hidden states 1, 0 the angles θ_1 and θ_2 are not independent, and we have $p_{10}(\theta_1, \theta_2) = p_{\theta_2|\theta_1=\theta_1}(\theta_2)$. Note we have assumed that we can observe the previous angle change directly, which is equivalent to assuming that the pattern of hidden states was in fact 0, 1, 0.

The remaining cases involve reorientation events in successive time intervals. Suppose we have the case where we have two successive reorientation events, giving a pattern of hidden states 1, 1, which is shown graphically in Fig 4d). This case is similar to the case with hidden states 1, 0 (see Fig 4c)), in that we observe a contribution to the reorientation angle from the correction for the previous reorientation event, θ_2 , and also a contribution from the new reorientation event, θ'_1 . As can be seen in Fig 4d), these contributions sum together to give an observed angle change for the time interval $[k\Delta t, (k+1)\Delta t)$ of $\theta = \theta_2 + \theta'_1$. The probability density for sums of random variables can be expressed as a convolution [18]. Hence, $p_{11}(\theta_1, \theta) = (p_{\Theta_1} * p_{\Theta_2|\Theta_1=\theta_1})(\theta)$, where $*$ is the convolution operator. Any further cases involve multiple reorientation events within a single time interval which occurs rarely, with probability on the order of $\mathcal{O}((\lambda\Delta t)^2)$; we can neglect these provided $\lambda\Delta t \ll 1$.

To summarise therefore, the emission probabilities (that is the probability of observing a certain angle change given the sequence of hidden states) in the case without noise can be given as follows:

$$\begin{aligned} p_{00}(\theta) &= \delta(\theta); \\ p_{01}(\theta) &= p_{\Theta_1}(\theta); \\ p_{10}(\theta) &= p_{\Theta_2|\Theta_1}(\theta); \\ p_{11}(\theta) &= (p_{\Theta_2|\Theta_1} * p_{\Theta'})(\theta). \end{aligned}$$

Model with measurement noise

To account for noise, we introduce another layer of states in our diagram of state dependencies, as shown in Fig 3c). Let z_k be the noisy observed angle change at time $k\Delta t$, which is a noisy observation of θ_k , such that for a noise model, K , we have $z_k \sim K(\cdot, \theta_k)$. Alternatively, we can write the noisy observed angle as

$$z_k = \theta_k + \epsilon_k, \tag{3}$$

where $\epsilon_k \sim K(\cdot, 0)$. Under the assumption of a wrapped normal noise model, we obtain $\epsilon_k \sim N(0, \sigma^2)$. Since Eq (3) represents z_k as a sum of random variables, it becomes clear that we can obtain the noisy emission probabilities, q_{ij} , corresponding to a pattern of hidden states i, j via the following convolution:

$$q_{ij}(\theta) = (p_{ij} * K)(\theta) = \int_{\Theta} p_{ij}(\theta - x)K(x, 0)dx.$$

To extend our previous results to the noisy case, we therefore need to compute these convolutions, a task that must be carried out numerically.

Derivation of emission probabilities

In previous work [33], marginal distributions for the observed angle change, Θ_1 , were obtained and we summarise the arguments here. Fig 5 shows the true angle change and the observed angle change based on discrete time observations of the VJP.

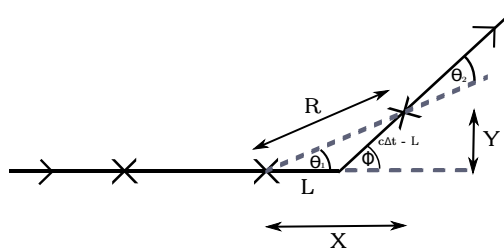


Fig 5. True and observed angle changes based on discrete time observations of a VJP without measurement error. Cartesian co-ordinates X and Y are shown in addition to polar co-ordinates R and Θ_1 . The object is moving along the trajectory from left to right as shown by the arrows.

By changing co-ordinates from the displacement, L , (which is given by the running time distribution f_τ) and true angle change, Φ , to Cartesian co-ordinates, and then to polar co-ordinates, R and Θ_1 , we can obtain a joint distribution for R and Θ_1 of

$$f_{R, \Theta_1}(r, \theta_1) = \begin{cases} \frac{r}{c\Delta t(c\Delta t - r \cos \theta_1)} f_\Phi \left(\arccos \left[\frac{r^2 \sin^2 \theta_1 - (c\Delta t - r \cos \theta_1)^2}{r^2 \sin^2 \theta_1 + (c\Delta t - r \cos \theta_1)^2} \right] \right), & \text{if } (r, \theta_1) \in C; \\ 0, & \text{otherwise,} \end{cases}$$

where $C = \{r \leq c\Delta t, \theta \in [-\pi, \pi]\}$ is the set of permissible values for r and θ , Δt is the

discretisation in time and c is the running speed. Integrating $f_{R,\Theta_1}(r, \theta_1)$ over r allows us to obtain the marginal distribution for θ_1 via

$$f_{\Theta_1}(\theta_1) = \int_0^\infty f_{R,\Theta_1}(r, \theta_1) dr.$$

In the case where we assume a uniform reorientation kernel, $f_\Phi(\theta) = \mathbb{1}_{[-\pi,\pi]}(\theta)$, then this integral becomes

$$\begin{aligned} f_{\Theta_1}(\theta_1) &= \int_0^{c\Delta t} \frac{r}{2\pi c\Delta t(c\Delta t - r \cos \theta_1)} dr \\ &= \frac{-1}{2\pi c\Delta t \cos(\theta_1)} \int_0^{c\Delta t} \left(1 + \frac{\frac{c\Delta t}{\cos \theta_1}}{r - \frac{c\Delta t}{\cos \theta_1}} \right) dr \\ &= \frac{-1}{2\pi c\Delta t \cos(\theta_1)} \left[r + \frac{c\Delta t}{\cos \theta_1} \log \left| r - \frac{c\Delta t}{\cos \theta_1} \right| \right]_0^{c\Delta t} \\ &= \frac{-1}{2\pi \cos^2 \theta_1} (\cos \theta_1 + \log(1 - \cos \theta_1)). \end{aligned}$$

We note that the marginal distribution for θ_1 does not depend on the speed, c , or the time discretisation, Δt . This is intuitive because f_{Θ_1} is the pdf of a certain observed angle change, θ_1 , given there was a reorientation in that interval, irrespective of the length of that interval.

Derivation of the joint distribution of Θ_1 and Θ_2

By considering the displacement in the X and Y directions during a time step, we have

$$\begin{aligned} R \cos(\theta_1) &= L + (c\Delta t - L) \cos(\Phi), \\ R \sin(\theta_1) &= (c\Delta t - L) \sin(\Phi). \end{aligned}$$

Dividing these expressions, we can relate θ_1 to L and Φ by

$$\tan(\theta_1) = \frac{(c\Delta t - L) \sin(\Phi)}{L + (c\Delta t - L) \cos(\Phi)}, \tag{4}$$

and rearranging this for L , we have

$$L = \frac{c\Delta t(\tan \Phi - \tan \theta_1)}{\tan \Phi + \tan \theta_1(\sec \Phi - 1)}.$$

Differentiating with respect to θ_1 , we obtain

$$\frac{\partial L}{\partial \theta_1} = \frac{-c\Delta t \sec^2 \theta_1}{\tan \Phi + \tan \theta_1 (\sec \Phi - 1)} - \frac{c\Delta t (\tan \Phi - \tan \theta_1) \sec^2 \theta_1 (\sec \Phi - 1)}{(\tan \Phi + \tan \theta_1 (\sec \Phi - 1))^2},$$

which can be simplified to give

$$\frac{\partial L}{\partial \theta_1} = \frac{-c\Delta t \sin \Phi}{(\sin \Phi \cos \theta_1 + \sin \theta_1 (1 - \cos \Phi))^2}.$$

To transform from coordinates (L, Φ) to coordinates (θ_1, Φ) , we can use the Jacobian $J_{L,\Phi}$, where

$$\det J_{L,\Phi} = \frac{\partial L}{\partial \theta_1} = \frac{-c\Delta t \sin \Phi}{(\sin \Phi \cos \theta_1 + \sin \theta_1 (1 - \cos \Phi))^2}. \quad (5)$$

Therefore the joint distribution of θ_1 and Φ is

$$f_{\Theta_1, \Phi}(\theta_1, \phi) = \begin{cases} \frac{|c\Delta t \sin \Phi|}{(\sin \Phi \cos \theta_1 + \sin \theta_1 (1 - \cos \Phi))^2} \cdot f_{\Phi}(\phi) \cdot \frac{1}{c\Delta t}, & \text{if } \theta_1, \phi \in C; \\ 0, & \text{otherwise.} \end{cases}$$

Under the assumption that Φ is uniform on $[-\pi, \pi)$, as described in the Section “Velocity jump process models”, such that $f_{\Phi}(\theta) = \mathbb{1}_{[-\pi, \pi)}(\theta)$, we have

$$f_{\Theta_1, \Phi}(\theta_1, \phi) = \begin{cases} \frac{|\sin \Phi|}{2\pi(\sin \Phi \cos \theta_1 + \sin \theta_1 (1 - \cos \Phi))^2}, & \text{if } \theta_1, \phi \in C; \\ 0, & \text{otherwise.} \end{cases} \quad (6)$$

Changing variables again to (θ_1, θ_2) , via $\Phi = \theta_1 + \theta_2$, we have

$$f_{\Theta_1, \Theta_2}(\theta_1, \theta_2) = \begin{cases} \frac{|\sin(\theta_1 + \theta_2)|}{2\pi(\sin(\theta_1 + \theta_2) \cos \theta_1 + \sin \theta_1 (1 - \cos(\theta_1 + \theta_2)))^2}, & \text{if } \theta_1, \theta_2 \in C; \\ 0, & \text{otherwise.} \end{cases} \quad (7)$$

From this joint distribution, we can then find the conditional distribution of θ_2 given θ_1 , which is required to give $p_{10}(\theta) = f_{\Theta_1, \Theta_2}(\theta_1, \theta) / f_{\Theta_1}(\theta_1)$.

Approximate Bayesian computation

An alternative method commonly used for parameter estimation for models with intractable likelihoods is approximate Bayesian computation, or ABC [4, 30]. Suppose we can simulate data from a generative model, $x \sim g(x|\theta)$. An example would be simulating a path from our VJP model. To generate samples from the posterior distribution, we repeatedly generate parameters from the prior, $\theta \sim \pi(\theta)$, and use these parameters in our model to simulate synthetic data, $x \sim g(x|\theta)$. We compare the simulated data with the true observed data and, if it is close enough, we accept the sampled parameter as samples from the posterior. In cases where the data are discrete, we can consider whether simulated data, x , are equal to observed data, y , and accept parameters correspondingly, which gives samples exactly from the posterior. Often, though, our models are continuous and the acceptance rate from an exact comparison would be prohibitively small. Instead we can take a distance function and consider when the distance between x and y is within a chosen tolerance ϵ , that is $d(x, y) < \epsilon$. This introduces an approximation, which is exact only in the limit $\epsilon \rightarrow 0$. In practice, datasets can be high dimensional, resulting in very low acceptance rates for simulated data. By using summary statistics instead of the full datasets, we can reduce the dimensionality and obtain higher acceptance rates. Using summary statistics introduces another approximation into the method, meaning we compare $d(s(x), s(y)) < \epsilon$, where $s(x)$ gives the summary statistics for dataset x . We present the ABC method in Algorithm 3, and will show a comparison between application of pMCMC and ABC for parameter estimation of a VJP model based on time series data.

Algorithm 3 ABC rejection sampling

- 1: Sample parameter value θ from the prior $\pi(\theta)$.
 - 2: Generate synthetic dataset from the model $x \sim g(x|\theta)$.
 - 3: Accept sample θ if $d(s(x), s(y)) < \epsilon$, for a distance function, $d(\cdot, \cdot)$, summary statistics, $s(\cdot)$, and tolerance ϵ .
-

Results

We are able to investigate the effects of experimental design such as the discretisation, Δt , of a time series on the estimated biophysical parameters, using the framework for

inferring the parameters of a VJP described in the Section “Methods”. We demonstrate the effects of restrictions imposed by experimental constraints on a trade-off between discretisation in time versus measurement noise. As such our results can be used to provide guidance for experimental design choices.

Increasing Δt results in an abrupt break down in the posterior

We first assume that the magnitude of the noise on the observed angle, σ , is fixed. We vary the sampling frequency used to collect the data (corresponding to using different values of Δt). We generate observed (in silico) data by simulating one single trajectory directly from the VJP model, discretise this to generate observed angle changes with a temporal resolution of Δt , and add independent Gaussian noise with zero mean and variance σ^2 to these observations, representing measurement noise. Using datasets generated from the same simulated path discretised at different temporal resolutions, Δt , as shown in Fig 6, we infer a posterior distribution for the reorientation rate, λ , of the VJP model and the magnitude of the measurement noise, σ , via particle MCMC.

We use a Metropolis-Hastings algorithm to run the MCMC algorithm with a bootstrap particle filter [17] using 400 particles to provide an estimate of the likelihood. As a proposal distribution, we use the kernel $K(\cdot, \theta) \sim N(\theta, \Sigma)$, where

$$\Sigma = \begin{bmatrix} 0.5 & 0 \\ 0 & 0.05 \end{bmatrix}.$$

We run the Markov chain for $N = 50,000$ steps with thinning of $m = 2$. The prior is uniform on the log of the parameters over the intervals $[-1.70, 1.30]$ and $[-5, 1]$ for λ and σ , respectively. The results are shown in Fig 7 for $\Delta t = 1/8, 1/4, 1/2, 1, 2, 4, 8$ seconds, with noise of unknown magnitude σ , where here $\sigma = 0.04$ rad. We obtain samples from the posterior distributions that are very similar for small Δt , and observe an abrupt break down in the posterior distributions obtained for datasets sampled at larger values of Δt . This break down in posterior quality arises for values of $\Delta t \geq 2$ s, when multiple reorientation events in a time interval start to become more common (see also Fig 13). Provided that Δt and λ are such that the probability of multiple reorientations in a time interval is small, we obtain accurate estimates of the

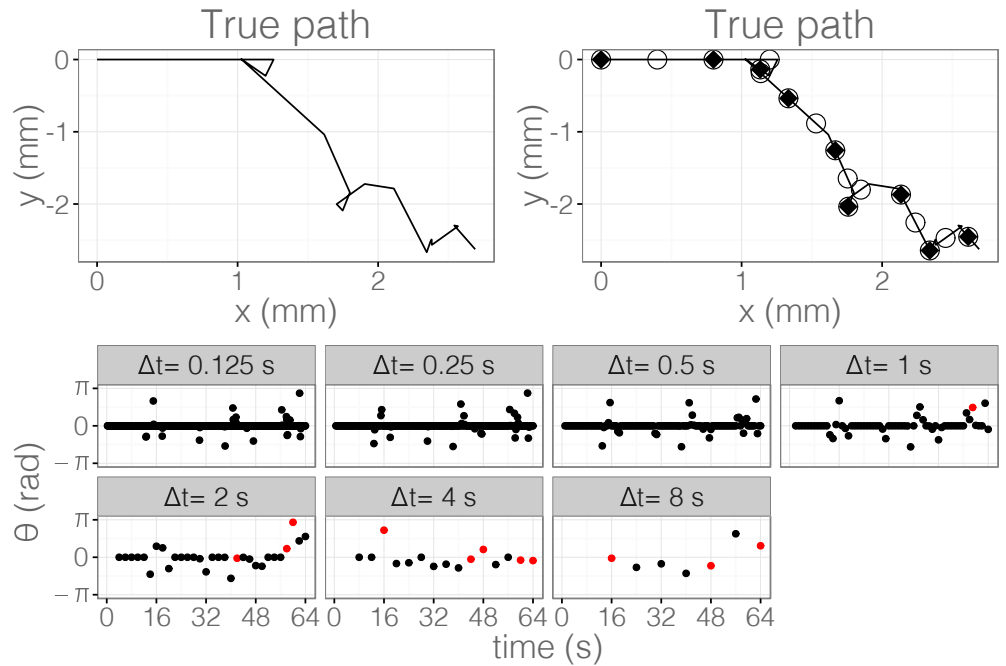


Fig 6. The data used in the pMCMC inference discretised at differing resolutions. The true trajectory is shown without discretisation in the first row, alongside the same path with circle markers to show the observed positions with $\Delta t = 4$ s and filled triangular markers to show observed positions with $\Delta t = 8$ s. The corresponding observed angle changes are shown the the lower rows for different values of Δt . Observations corresponding to multiple reorientations in a single time interval are highlighted in red. Parameters used in generating these data were a reorientation rate of $\lambda = 0.2\text{s}^{-1}$, a run speed of $c = 50\mu\text{ms}^{-1}$ and a total duration of observation of $T = 64$ s. A circular uniform distribution was used for the reorientation kernel. Observations are shown without measurement noise.

joint posterior distribution for the model parameters.

Increasing σ increases the variance of the posterior for λ

To investigate sensitivity of the posterior to measurement noise, we now fix the discretisation, Δt , and vary the measurement noise amplitude, σ , used to create each dataset. Applying the same analysis as in the previous subsection, for a fixed value of $\Delta t = 2$, we obtain posterior distributions for the reorientation rate, λ , and measurement noise, σ , as shown in Fig 7. We find that increasing the noise amplitude, σ , increases the variance in the posterior distribution obtained for the reorientation rate, λ . In addition, we are able to correctly estimate the value of σ used to generate the datasets.

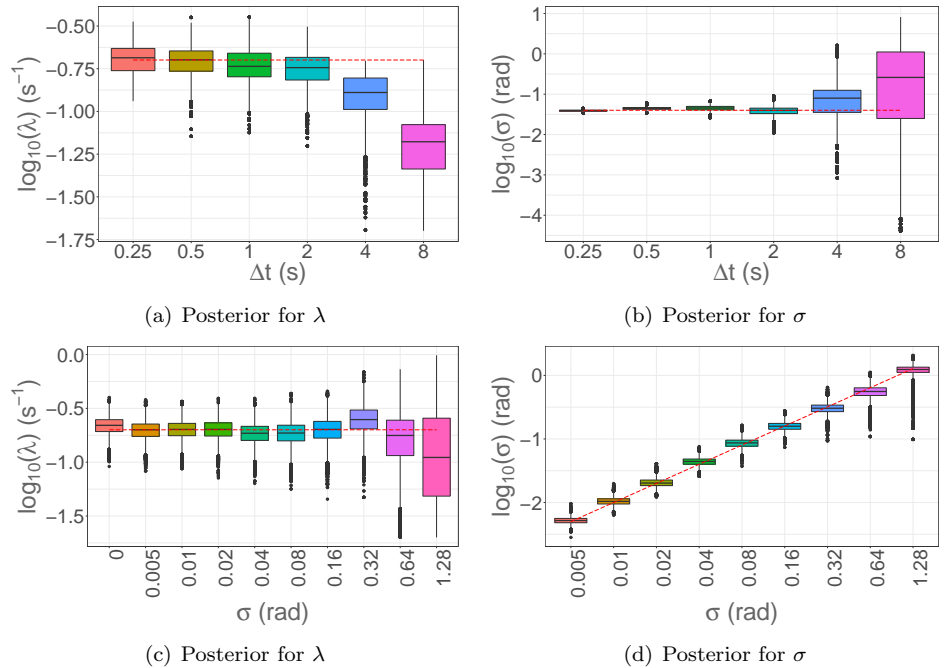


Fig 7. Results of parameter estimation via pMCMC for the reorientation rate, λ , and measurement noise, σ . Data collected with different values of Δt and fixed measurement noise, $\sigma = 0.04$ rad, were used in (a) and (b). Data generated with a fixed value of $\Delta t = 1$ s and different values of the measurement noise, σ , were used in (c) and (d). The marginal posterior distributions for λ are given in (a) and (c), while the marginal posterior distributions for σ are shown in (b) and (d). The red dashed lines indicate the true values of parameters used in simulation of the datasets. The central rectangle of each boxplot shows the quartiles of the plotted distribution, with the central line giving the median. The whiskers above and below the rectangle show the maximum and minimum of the distribution unless there are outliers beyond 1.5 times the interquartile range below or above the 1st or 3rd quartiles, which are shown as dots.

We note that the presence of noise in the datasets results in a bias towards smaller estimates of the reorientation rate, λ . This can be explained intuitively by reasoning that some reorientations leading to very small observed angle changes are mistaken for noise as σ increases.

More data provides better estimates

Let T be the total duration of our observations of the system. For a fixed value of the time discretisation, Δt , varying T is equivalent to gathering a bigger dataset. We fix $\Delta t = 1$ s and allow T to vary so that we can consider the effects of collecting more data. Posteriors for the reorientation rate, λ , are shown in Fig 8.

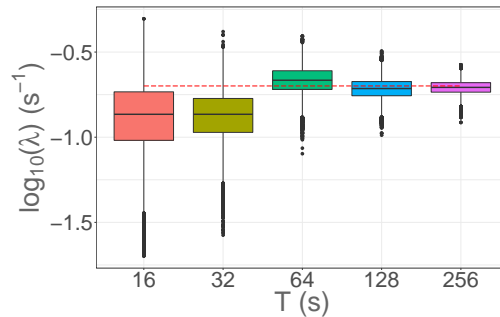


Fig 8. Results of parameter estimation via pMCMC for the reorientation rate, λ , with $\Delta t = 1$ s and $\sigma = 0$ rad, whilst varying T to give different sized datasets.

It is clear that larger datasets result in less bias and less variance for estimates of the reorientation rate, λ . However, we note that running the particle filter within the pMCMC algorithm becomes much more computationally intensive as the size of the dataset increases, scaling as $\mathcal{O}(T)$ as the size of the dataset increases.

Experimental constraints

We investigate the implications of these results for experimental design, by considering an imaging experiment to observe the position of an object of interest (for example, a bacterium) at regular time points. The behaviour of our system of interest happens over a certain timescale inherent to the biological process, so we fix the total duration for the imaging experiment, T , based on this timescale. We consider how best to choose the time between successive observations, Δt , given the restriction of a fixed photon budget. That is, we assume that the biological sample can only be exposed to a fixed number of photons before phototoxicity or photobleaching significantly reduce the quality of, or destroy, any further potential data. The results of Zhao et al. [41] suggest that there is an inverse square relationship between the signal to noise ratio (SNR) and the time between successive frames, Δt , of the form

$$\text{SNR} = \frac{k}{\sqrt{\Delta t}}, \quad (8)$$

where k is a constant that depends on the imaging set up, but not other experimental design choices. Assuming that for our model the noise is of magnitude σ , we find an

inverse square relationship between σ and Δt , such that

$$\sigma = \frac{K}{\sqrt{\Delta t}}, \tag{9}$$

for a new constant K which is k times the average angle change.

To investigate how to choose Δt given a fixed photon budget, we set a value of the proportionality constant and vary σ and Δt according to this relationship. We take proportionality constants $K = 0.08$ and $K = 0.8$ in Fig 9. A larger value of the proportionality constant, K , corresponds to worse imaging conditions, in that for a fixed value of Δt , the noise in the images obtained will be greater. Therefore we expect our inference method to perform worse for a larger value of K . We then ask the question, for a given value of K , how should we choose Δt to improve the parameter estimation? Our results in Fig 9 suggest that the value of Δt should be taken as small as possible, even if this increases the noise present in the data.

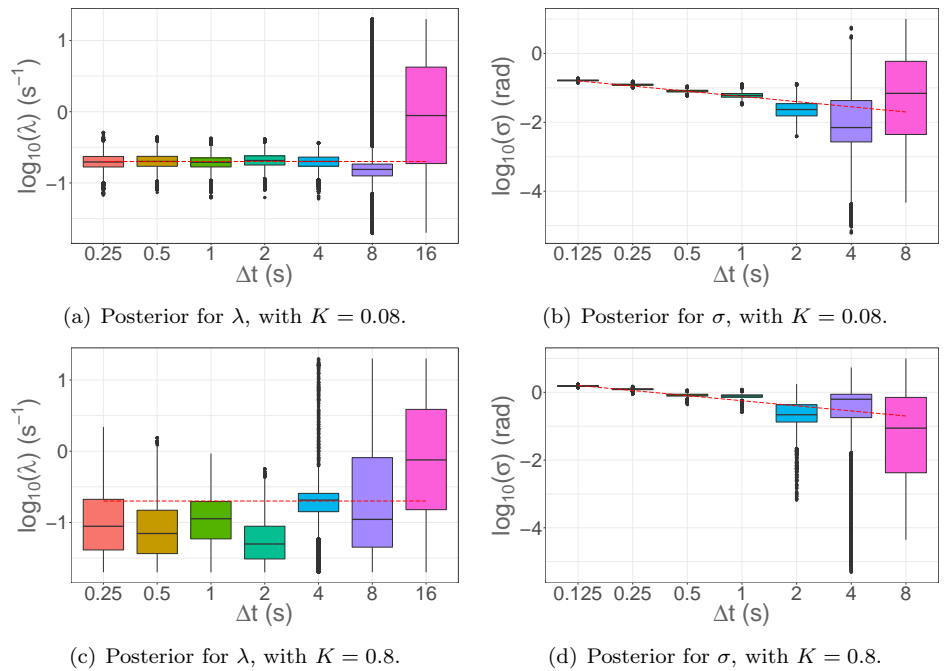


Fig 9. Results of parameter estimation via pMCMC for the reorientation rate, λ , and measurement noise, σ , using data generated with a fixed value of Δt and different values of the measurement noise, σ . We have varied both σ and Δt with an inverse square root relationship between these, as in Eq.(9). The posterior distributions for λ are given in (a) and (c), while the posterior distributions for σ are shown in (b) and (d). The proportionality constant is $K = 0.08$ for (a) and (b), and $K = 0.8$ for (c) and (d).

Comparison to approximate Bayesian computation

A common approach for mathematical and computational models where the likelihood is intractable is to apply ABC for parameter inference [4, 30]. Although ABC produces samples from an approximate posterior, rather than the exact posterior distribution, it is intuitively simple to understand and implement. ABC methods have been applied to parameter estimation for biased, persistent random walk models very similar to our VJP model [19, 22, 35, 40]. For these methods, the choice of which summary statistics to use has notable effects on the approximate posterior distributions obtained via ABC.

We compare the quality of resulting posterior distributions obtainable with ABC to those from pMCMC. Our results, shown in Fig 10, suggest that for small values of Δt , when the dimensionality of the data observed is high, ABC performs poorly at approximating the posterior for the parameters of our VJP, which we were able to sample exactly using pMCMC. However, for large values of Δt , when we have a low dimensional dataset, ABC produces an approximate posterior centred on the true reorientation rate, λ , although it fails to capture the tails of the true posterior, with far too much concentration of the posterior samples around the true value. In addition, since the inference procedure in this case is not dependent on assumptions about multiple reorientations in a time step, we do not see a deterioration in the quality of the approximate posterior distributions as Δt increases.

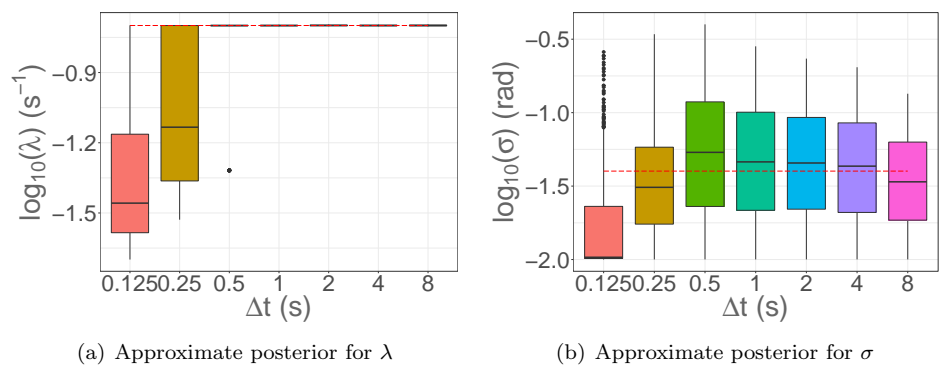


Fig 10. Parameter estimation via ABC rejection sampling for the reorientation rate, λ , in (a), and the measurement noise, σ , in (b), using full time series data collected with noise of magnitude $\sigma = 0.04$ rad, for different values of Δt . $N = 500,000$ datasets were generated and parameter samples corresponding to the closest 0.1% of the datasets were retained to give the approximate posterior.

For the results in Fig 10, we use the full available dataset consisting of observed angle changes at each time point. We generate $N = 500,000$ synthetic datasets based on parameters sampled from the prior, calculate the Euclidean distance between these synthetic datasets and our observed data, and select the parameters corresponding to 0.1% of the datasets closest to the observed data. As previously, we take a duration of time series $T = 64$ s, and a prior uniform on the log of the parameters on the intervals $[-1.70, 1.30]$ and $[-2, 1]$ for λ and σ , respectively.

We consider also the effects on the approximate posteriors sampled via ABC of using summary statistics, such as the transition matrices described in Jones et al. [19], which enable us to reduce the dimensionality of the data. A transition matrix allows us to summarise time series data via a two-dimensional binning of the observed angles, based on the current observed angle change and the previous observed angle change. We bin the observed angle time series data into an n by n matrix, where $n = 5$, and use this as our summary statistic. This provides a much lower dimensional summary of the data for the smaller values of Δt , although for large values of Δt , we may end up with higher dimensional (sparse) data, as in this case there will be fewer than n^2 observations. As a result, the approximate posteriors for small Δt provide better estimates of the true reorientation rate and are much closer to the true posterior, as shown in Fig 11. However, this method of summarising the data offers limited information about the measurement noise, σ . This issue could be mitigated by increasing n to give a finer discretisation of the angles (which would require sufficient data), or by targeting the noise with an additional summary statistic. Using the transition matrix summary statistics gives similar performance to ABC on the full dataset for large values of Δt , since by taking the summary statistic in this case we are increasing the dimensionality of the data without adding any extra information.

To obtain potentially improved results for inference with ABC for this type of data, we could consider a more systematic choice of summary statistics [3, 8, 14] or a more efficient version of the ABC algorithm, such as ABC-SMC [34, 37], which applies importance sampling. Other improvements could be possible by applying a regression adjustment, via linear regression [4] or using nonlinear regression techniques such as with a neural network [7].

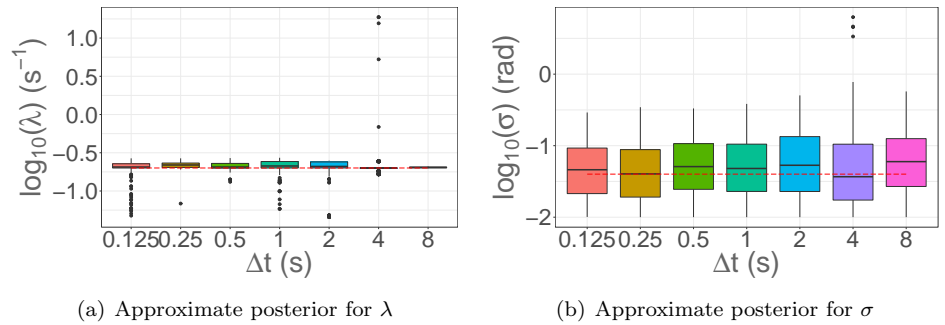


Fig 11. Parameter estimation via ABC rejection sampling for the reorientation rate, λ , in (a), and the measurement noise, σ , in (b), using transition matrix summary statistics collected with noise of magnitude $\sigma = 0.04$ rad on the observed angles, for different values of Δt . $N = 500,000$ datasets were generated and parameter samples corresponding to the closest 0.1% of the datasets were retained to give the approximate posterior.

Discussion

In this work, we have considered parameter estimation of a VJP model for biological transport and how insights from this inference can inform experimental design. We have considered estimation of posterior distributions for parameters of a VJP model based on noisy datasets collected at varying temporal resolutions. To perform this parameter inference, we used pMCMC and derived the appropriate emission probabilities. We observed an abrupt break down in the quality of the posteriors obtained when increasing the discretisation in time. This transition corresponds to a break down in modelling assumptions underlying the derivation of the emission probabilities. For example, as Δt increases we see multiple reorientations in a time interval.

Increasing the magnitude of the noise in the data slowly decreased the quality of the median posterior estimates and increased the posterior variance. In general, better estimates were obtained when more data was available, either by decreasing Δt , or by increasing the total duration of the observations, T . We also compared parameter estimation with pMCMC to that with ABC, which suggested that different methods are appropriate in different situations, dependent on the data available. In particular, pMCMC performs well provided the assumptions made in deriving the emission probabilities hold, which is true for small Δt . For larger values of Δt , ABC would be a better choice than pMCMC as it does not require the same modelling assumptions as

pMCMC. Using the full time series dataset is preferred if the dimensionality of the observed data is low, but for high dimensional data, using summary statistics such as the transition matrix will give higher acceptance rates in ABC.

Through comparison between inference with pMCMC and ABC, our results highlight a weakness of inference with ABC, in that it performs poorly for high dimensional data, and also a weakness of our application of pMCMC, which is that it relies upon assumptions about the number of reorientation events in a time step; when this fails our posterior estimates are no longer accurate. We note, additionally, that pMCMC allows us to sample from the exact posterior for parameters from a model (given that model is appropriate to describe the data), whereas via ABC we obtain approximate posteriors for a fixed tolerance, ϵ , which only become exact in the limit as $\epsilon \rightarrow 0$.

In Section “Methods”, we described a framework for inference using pMCMC, and made certain assumptions about the VJP model, such as a separation in timescales between runs and reorientations, and a memoryless exponential distribution for the running time. Although many of these are standard assumptions, it would be possible to perform the same analysis in a more general model. For instance, if a running time distribution was chosen that does not satisfy the memoryless property, we could introduce an extra hidden variable, s , for the time since the last reorientation. In addition, in this work we have described parameter estimation via a hidden states formulation of the VJP model using dependence on hidden states from two time intervals. This can be extended to hidden states from three time intervals, which can allow rare consecutive reorientation events to be handled more accurately albeit at greater computational cost.

Given a fixed photon budget and a trade-off between temporal sampling frequency and measurement noise, our results in the Section “Experimental constraints” indicate that a small value of Δt should be used for the discretisation in time i.e. that motile individuals should be imaged as frequently as possible. In practice, there may be disadvantages to this choice of Δt . Computationally, the parameter inference via pMCMC will be significantly more computationally expensive, although the computational run time may still be small in comparison to the duration of an experimental protocol. Datasets with much higher noise present may also be much

harder to interpret. Here, we have assumed that the noise present in the data is applied to the observed angle change. In reality there is noise on each pixel, which may contribute to an uncertainty in identifying the observed position of the object of interest.

Acknowledgements

This work was supported by funding from the Engineering and Physical Sciences Research Council (EPSRC) (grant no. EP/G03706X/1). REB is a Royal Society Wolfson Research Merit Award holder, and would like to thank the Leverhulme Trust for a Leverhulme Research Fellowship.

S1 Appendix

Comparison with simulations

To verify our emission probabilities calculated in the Section “Derivation of emission probabilities”, we can compare the distributions of observed angle changes from simulations with those predicted theoretically. We simulate from the VJP model for a known pattern of hidden states and assume no measurement noise is present.

Performing these checks for hidden states of the form $0, 1$, we obtain results as shown in Fig 12(a); there is excellent agreement between simulation and theory which verifies our theoretical results. For hidden states of the form $1, 0$, we must condition on the value of the previous angle change. We demonstrate agreement between the theory and simulations, for different values of the previous angle change, in Fig 12(b).

Similarly, we show corresponding results for hidden states of the form $1, 1$ in Fig 12(c).

Supporting information

S1 Appendix. Comparison with simulations. Comparison of the analytic form for the emission probabilities with results from simulated paths.

S2 Fig. Probability of hidden state sequences. Probability of sequences of hidden states as Δt varies, showing where multiple reorientations in a time interval appear as Δt increases.

S3 Code Code implementing Bayesian inference via pMCMC for a VJP model. Example code to implement pMCMC for a VJP model, as described in Section “Methods”, is available at https://github.com/shug3502/pmmc_inference_for_vjps

References

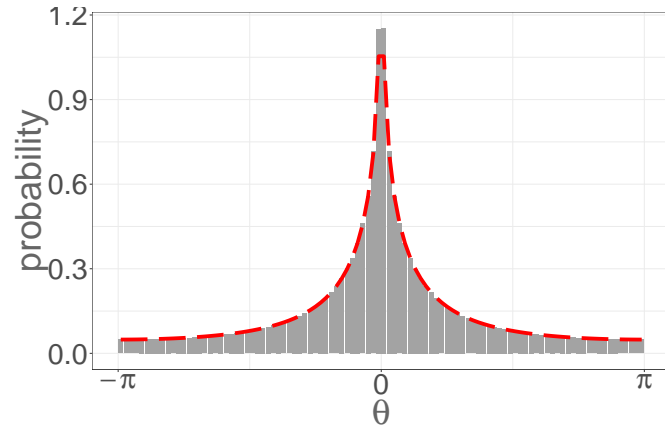
1. C Andrieu and G O Roberts. The pseudo-marginal approach for efficient Monte Carlo computations. *The Annals of Statistics*, 37(2):697–725, 2009.
2. C Andrieu, A Doucet, and R Holenstein. Particle Markov chain Monte Carlo methods. *Journal of the Royal Statistical Society: Series B*, 72(3):269–342, 2010.
3. C Barnes, S Filippi, M P H Stumpf, and T Thorne. Considerate approaches to constructing summary statistics for ABC model selection. *Statistics and Computing*, 22(6):1181–1197, 2012.
4. M A Beaumont, W Zhang, and D J Balding. Approximate Bayesian computation in population genetics. *Genetics*, 162(4):2025–2035, 2002.
5. S Benhamou. How many animals really do the Lévy walk? *Ecology*, 88(8):1962–1969, 2007.
6. H C Berg and D A Brown. Chemotaxis in *Escherichia coli* analysed by three-dimensional tracking. *Nature*, 239(5374):500–504, 1972.
7. M G Blum and O François. Non-linear regression models for approximate Bayesian computation. *Statistics and Computing*, 20(1):63–73, 2010.
8. M G Blum, M A Nunes, D Prangle, and S A Sisson. A comparative review of dimension reduction methods in approximate Bayesian computation. *Statistical Science*, 28(2):189–208, 2013.

9. P Bovet and S Benhamou. Spatial analysis of animals' movements using a correlated random walk model. *Journal of Theoretical Biology*, 131(4):419–433, 1988.
10. E A Codling and N A Hill. Calculating spatial statistics for velocity jump processes with experimentally observed reorientation parameters. *Journal of Mathematical Biology*, 51(5):527–556, 2005.
11. E A Codling, M J Plank, and S Benhamou. Random walk models in biology. *Journal of the Royal Society Interface*, 5(25):813–834, 2008.
12. A Doucet, S Godsill, and C Andrieu. On sequential Monte Carlo sampling methods for Bayesian filtering. *Statistics and Computing*, 10(3):197–208, 2000.
13. A M Edwards, R A Phillips, N W Watkins, M P Freeman, E J Murphy, V Afanasyev, S V Buldyrev, M G da Luz, E P Raposo, and H E Stanley. Revisiting Lévy flight search patterns of wandering albatrosses, bumblebees and deer. *Nature*, 449(7165):1044–1048, 2007.
14. P Fearnhead and D Prangle. Constructing summary statistics for approximate Bayesian computation: semi-automatic approximate Bayesian computation. *Journal of the Royal Statistical Society: Series B*, 74(3):419–474, 2012.
15. A Golightly and D J Wilkinson. Bayesian parameter inference for stochastic biochemical network models using particle Markov chain Monte Carlo. *Interface Focus*, 1(6):807, 2011.
16. A Golightly, D A Henderson, and C Sherlock. Delayed acceptance particle MCMC for exact inference in stochastic kinetic models. *Statistics and Computing*, 25(5):1039–1055, 2015.
17. N J Gordon, D J Salmond, and A F Smith. Novel approach to nonlinear non-Gaussian Bayesian state estimation. *IEE Proceedings F*, 140(2):107–113, 1993.
18. G Grimmett and D Stirzaker. *Probability and Random Processes*. Oxford University Press, 2001.

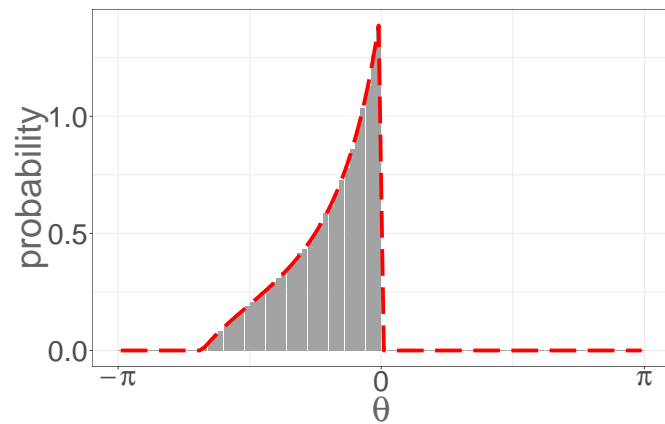
19. P Jones, A Sim, H Taylor, L Bugeon, M Dallman, B Pereira, M P H Stumpf, and J Liepe. Inference of random walk models to describe leukocyte migration. *Physical Biology*, 12(6):66001–66012, 2015.
20. I D Jonsen, J M Flemming, and R A Myers. Robust state-space modeling of animal movement data. *Ecology*, 86(11):2874–2880, 2005.
21. PM Kareiva and N Shigesada. Analyzing insect movement as a correlated random walk. *Oecologia*, 56(2):234–238, 1983.
22. J Liepe, H Taylor, C Barnes, M Huvet, L Bugeon, T Thorne, J Lamb, M Dallman, and M P H Stumpf. Calibrating spatio-temporal models of leukocyte dynamics against in vivo live-imaging data using approximate Bayesian computation. *Integrative Biology*, 4(3):335–345, 2012.
23. J T Mandeville, R N Ghosh, and F R Maxfield. Intracellular calcium levels correlate with speed and persistent forward motion in migrating neutrophils. *Biophysical Journal*, 68(4):1207–1217, 1995.
24. A Nicosia, T Duchesne, L P Rivest, and D Fortin. A general hidden state random walk model for animal movement. *Computational Statistics and Data Analysis*, 105:76–95, 2017.
25. H G Othmer, S R Dunbar, and W Alt. Models of dispersal in biological systems. *Journal of Mathematical Biology*, 26(3):263–298, 1988.
26. H G Othmer and T Hillen. The diffusion limit of transport equations derived from velocity-jump processes. *SIAM Journal on Applied Mathematics*, 61(3):751–775, 2000.
27. K J Painter. Modelling cell migration strategies in the extracellular matrix. *Journal of Mathematical Biology*, 58(4):511–543, 2009.
28. R Pankov, Y Endo, S Even-Ram, M Araki, K Clark, E Cukierman, K Matsumoto, and K M Yamada. A Rac switch regulates random versus directionally persistent cell migration. *Journal of Cell Biology*, 170(5):793–802, 2005.

29. R M Parton, A Davidson, I Davis, and T T Weil. Subcellular mRNA localisation at a glance. *Journal of Cell Science*, 127(10):2127–2133, 2014.
30. J K Pritchard, M T Seielstad, A Perez-Lezaun, and M W Feldman. Population growth of human Y chromosomes: a study of Y chromosome microsatellites. *Molecular Biology and Evolution*, 16(12):1791–1798, 1999.
31. D A Rasmussen, O Ratmann, and K Koelle. Inference for nonlinear epidemiological models using genealogies and time series. *PLOS Computational Biology*, 7(8):e1002136, 2011.
32. G Rosser, A G Fletcher, D A Wilkinson, J A de Beyer, C A Yates, J P Armitage, P K Maini, and R E Baker. Novel methods for analysing bacterial tracks reveal persistence in *Rhodobacter sphaeroides*. *PLOS Computational Biology*, 9(10):1:18, 2013.
33. G Rosser. *Mathematical modelling and analysis of aspects of planktonic bacterial motility*. PhD thesis, University of Oxford, 2012.
34. S A Sisson, Y Fan, and M M Tanaka. Sequential Monte Carlo without likelihoods. *Proceedings of the National Academy of Sciences*, 104(6):1760–1765, 2007.
35. H B Taylor, J Liepe, C Barthen, L Bugeon, M Huvet, P W Kirk, S B Brown, J R Lamb, M P H Stumpf, and M Dallman. P38 and JNK have opposing effects on persistence of in vivo leukocyte migration in zebrafish. *Immunology and Cell Biology*, 91(1):60–69, 2013.
36. J P Taylor-King, E van Loon, G Rosser, and S J Chapman. From birds to bacteria: generalised velocity jump processes with resting states. *Bulletin of Mathematical Biology*, 77(7):1213–1236, 2015.
37. T Toni, D Welch, N Strelkova, A Ipsen, and M P H Stumpf. Approximate Bayesian computation scheme for parameter inference and model selection in dynamical systems. *Journal of the Royal Society Interface*, 6(31):187–202, 2009.

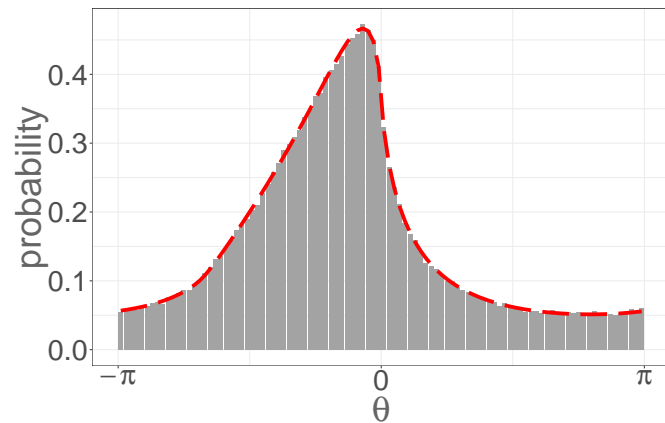
38. G M Viswanathan, V Afanasyev, S V Buldyrev, E J Murphy, P A Prince, and H E Stanley. Lévy flight search patterns of wandering albatrosses. *Nature*, 381 (6581):413–415, 1996.
39. G M Viswanathan, V Afanasyev, S V Buldyrev, S Havlin, M G Da Luz, E P Raposo, and H E Stanley. Lévy flights in random searches. *Physica A*, 282(1): 1–12, 2000.
40. H Weavers, J Liepe, A Sim, W Wood, P Martin, and M P H Stumpf. Systems analysis of the dynamic inflammatory response to tissue damage reveals spatiotemporal properties of the wound attractant gradient. *Current Biology*, 26 (15):1975–1989, 2016.
41. Q Zhao, I T Young, and J G De Jong. Photon budget analysis for fluorescence lifetime imaging microscopy. *Journal of Biomedical Optics*, 16(8): 086007–086007, 2011.



(a) Hidden states: 0,1



(b) Hidden states: 1,0



(c) Hidden states: 1,1

Fig 12. Comparison between simulated results and theoretical predictions of the observed angle change for hidden states of the form 0, 1 in (a), 1, 0 in (b), and 1, 1 in (c). The simulated results are shown by the histogram and the theoretical prediction for the observed angle change distribution is shown as the red dashed line. For both (b) and (c), we have conditioned on an observed angle change in the previous time interval of 0.1 rad, and for (c) we also conditioned on an observed angle change prior to that of -1.0 rad. To generate these results, we used $N = 10^7$ simulated trajectories with running speed $c = 50 \mu\text{ms}^{-1}$, uniform reorientation kernel, reorientation rate $\lambda = 0.2 \text{ s}^{-1}$ and time discretization $\Delta t = 1 \text{ s}$.

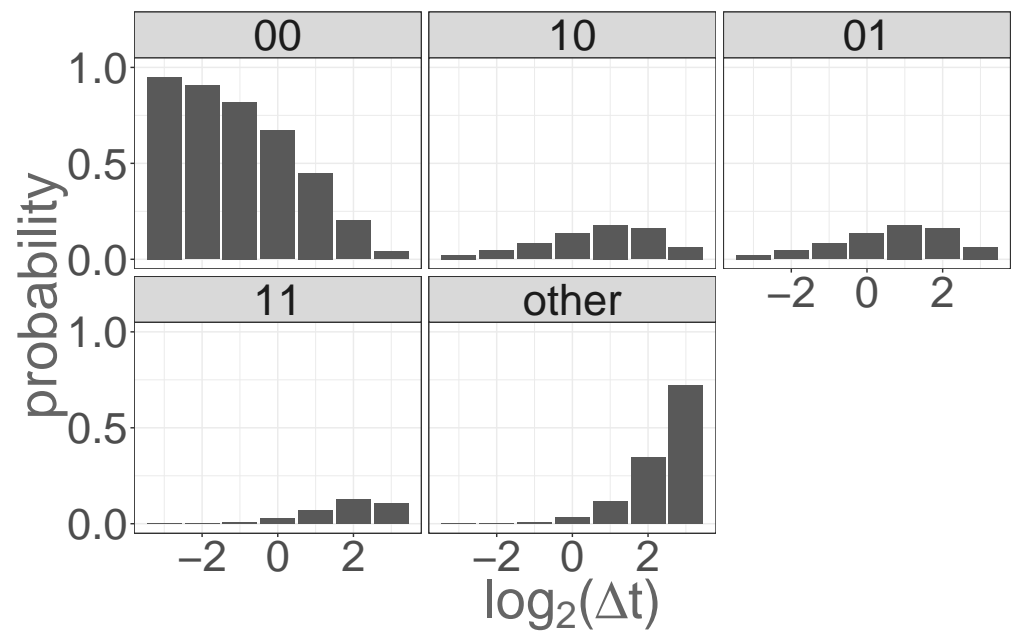


Fig 13. The probability of sequences of hidden states as Δt varies with reorientation rate $\lambda = 0.2 \text{ s}^{-1}$. For coarse values of Δt , the assumptions of the model start to break down as multiple reorientations appear within a single time interval.